

# International Conference on Space Optics—ICSO 2012

Ajaccio, Corse

9–12 October 2012

*Edited by Bruno Cugny, Errico Armandillo, and Nikos Karafolas*



## *Novel unimorph deformable mirror for space applications*

*Sven Verpoort*

*Peter Rausch*

*Ulrich Wittrock*



# Novel Unimorph Deformable Mirror for Space Applications

Sven Verpoort, Peter Rausch, and Ulrich Wittrock

Photonics Laboratory, Münster University of Applied Sciences  
Stegerwaldstraße 39, 48565 Steinfurt, Germany.

[verpoort@fh-muenster.de](mailto:verpoort@fh-muenster.de), [rausch@fh-muenster.de](mailto:rausch@fh-muenster.de), [wittrock@fh-muenster.de](mailto:wittrock@fh-muenster.de)

**Abstract** — We have developed a new type of unimorph deformable mirror, designed to correct for low-order Zernike modes. The mirror has a clear optical aperture of 50 mm combined with large peak-to-valley Zernike amplitudes of up to 35  $\mu\text{m}$ . Newly developed fabrication processes allow the use of prefabricated super-polished and coated glass substrates. The mirror's unique features suggest the use in several astronomical applications like the precompensation of atmospheric aberrations seen by laser beacons and the use in woofer-tweeter systems. Additionally, the design enables an efficient correction of the inevitable wavefront error imposed by the floppy structure of primary mirrors in future large space-based telescopes. We have modeled the mirror by using analytical as well as finite element models. We will present design, key features and manufacturing steps of the deformable mirror.

**Index Terms** — unimorph deformable mirror, aberration compensation, adaptive optics, active optics

## I. INTRODUCTION

Concepts for future ultra large space-based telescopes are based on light-weighted and composite primary mirrors which cannot meet the required optical surface figure. These primaries will generate several microns of wavefront error. To correct for these errors, deformable mirrors with sufficient stroke and high optical quality are required at some conjugate plane in the optical path. The mirror concept presented in this paper is based on a design originally developed for the correction of thermo-optical aberrations in high power laser systems. We have scaled this mirror design towards a clear optical aperture of 50 mm diameter to take into account the Lagrange invariant of large-aperture telescopes. The well matched thermal expansion coefficients of the mirror components shall allow the use of the mirror at temperatures down to 100 K.

The mirror's unique features also suggest its use in terrestrial astronomical applications. As the wavefront measurement error of a laser guide star (LGS) system is linearly proportional to the LGS spot size, the mirror can be used to compensate for the atmospheric aberrations seen by the laser beam during propagation. This would allow simultaneous pre-compensation and alignment of the LGS system.

The large stroke of our mirror also offers the possibility to use the deformable mirror in the science light path as a woofer in a woofer-tweeter system.

The low total integrated scattering of less than 0.01% should also permit operation of the deformable mirror in stellar coronagraphs searching for extrasolar planets.

Generally, deformable mirrors provide control of the wavefront of coherent and partially coherent light. Therefore, these mirrors are tools of great importance in nearly all fields of optical sciences such as astronomy, ophthalmology, and laser physics. In astronomy, for instance, time-dependant wavefront errors severely limit the performance of telescopes. Terrestrial telescopes suffer from aberrations caused by atmospheric turbulences. While space-based telescopes avoid those atmospheric disturbances, their light-weighted and therefore floppy primary mirrors may induce aberrations which vastly reduce the telescope performance [1]. In terrestrial telescopes, the use of deformable mirrors to overcome the atmospheric seeing limit is well established [2, 3], many types of deformable mirrors are commercially available [4, 5].

Our mirror differs from many other mirror concepts by several key features. The mirror structure consists of a thin glass mirror bonded onto a prefabricated piezoelectric ceramic disc. This very thin laminate structure enables larger stroke compared to other bimorph or unimorph mirrors. A stroke of several tens of microns can be achieved with a 1 mm thick laminate structure. A glass substrate is polished and dielectrically coated before being bonded to the piezo disc. This procedure guarantees highly reflective and extremely low scattering optical surfaces, which rival the best available passive optics. Reflectivities of more than 99.998%, paired with a surface roughness of less than 1.5  $\text{\AA}$  RMS are achieved by state-of-the-art sputtered dielectric coatings. Furthermore, an integrated monolithic tip-tilt functionality makes a separate tip-tilt stage obsolete.

The presented design is being developed in the course of a project funded by the European Space Agency. The goal of this project is to design, manufacture, and test a space qualified deformable mirror. Such a mirror has never been employed in space telescopes so far. Space environment imposes certain challenges to the mirror design in terms of heat management, mechanical stability, and operation in cryogenic vacuum environment. To meet all these requirements, a strict selection of materials along with the development of an adequate mechanical design and customized fabrication workflow is necessary. Design and material parameters are described in section 2.

Beside the correction of aberrations in telescopes, another potential field of application could be the correction of

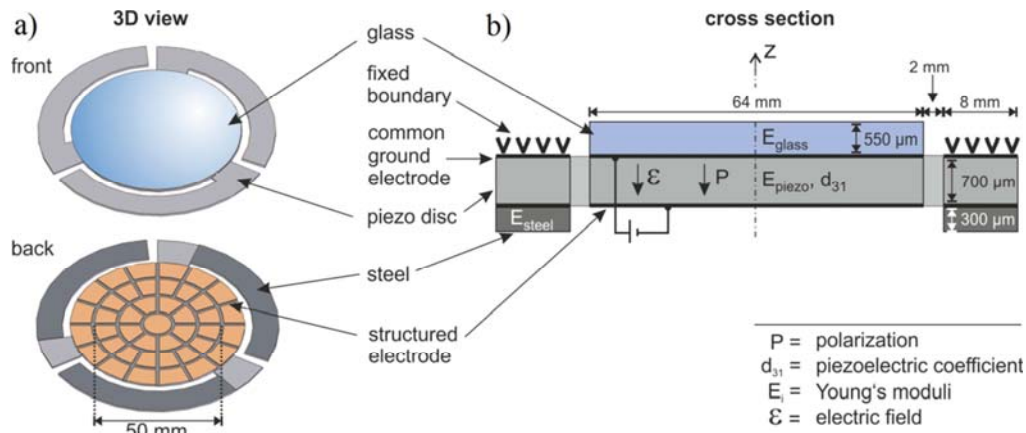


Fig. 1 a) Three-dimensional view of the deformable mirror along with the electrode pattern  
b) Cross-sectional view

thermally induced wavefront errors in high-power lasers. Powerful laser systems have become an important part in Earth observations missions, e.g. the laser of the Atmospheric Laser Doppler Instrument (ALADIN) for the ADM-Aeolus mission. One challenge is to maintain a good beam quality during the amplification process in such high-power systems. Here, an appropriately designed deformable mirror would help to improve the beam quality by compensating the detrimental aberrations.

## II. MIRROR DESIGN

Figure 1 shows a three-dimensional and a cross-sectional view of our mirror design. The mirror is based on a laser-cut three-arm piezoelectric disc which is sandwiched between two metallic electrodes. The unstructured front electrode serves as the common ground electrode while the structured back electrode is used to actuate the mirror. Structuring of the electrode as well as cutting of the piezo disc is done by cold ps-laser ablation to avoid any heat-affected zone.

If a voltage is applied to the electrodes, the piezo disc strains azimuthally and radially due to the reverse piezoelectric effect. The strain is proportional to the piezoelectric coefficient  $d_{31}$ . The induced lateral stress between the active piezo layer and the passive glass layer will cause a localized

deformation of the laminate in the area of the actuated electrode.

The back side electrode is subdivided into a 40-electrode keystone pattern plus one center electrode. 25 electrodes are within the 50 mm optical aperture and 16 electrodes form a ring surrounding the optical aperture. 3 additional electrodes actuate the arms. The geometry of this electrode pattern has been found by analytical calculations and was optimized by means of finite-element calculations [6]. It enables a reproduction of low-order Zernike modes with high stroke and high fidelity.

A dielectrically coated, super-polished glass substrate (see Fig. 2) is adhesively bonded to the front side of the piezo disc. The surface figure of the coated substrate has been investigated with a phase-stepping interferometer. The results presented in Fig. 3a) show a very small mainly spherical residual deformation of  $0.44 \mu\text{m}$  RMS. As can be seen in Fig. 3b), the deviation is only  $0.05 \mu\text{m}$  RMS at best defocus.

To bond the glass and piezo disc we use a low-outgassing UV-curable adhesive to meet the strict outgassing specifications as per ESA ECSS-Q-70. Advantageous in terms of outgassing is the extremely small free surface of the adhesive layer. Outgassing can only occur around the circumference of the mirror structure where the resulting free surface is approximately  $3 \text{ mm}^2$ .

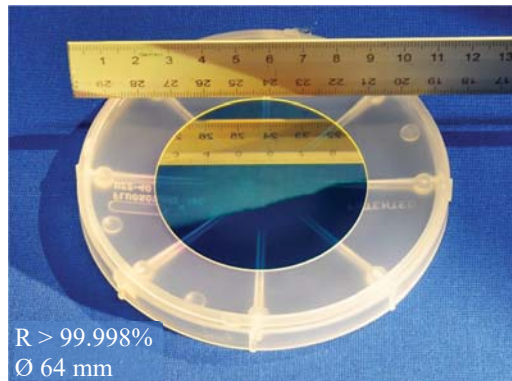


Fig. 2 HR-coated glass substrate ( $R > 99.998\%$  @ 1030 nm)

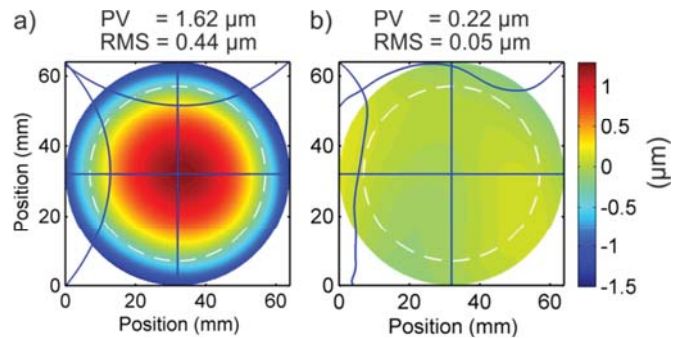


Fig. 3 Initial deformation of the coated glass substrate  
a) total deformation b) residual deformation at best defocus

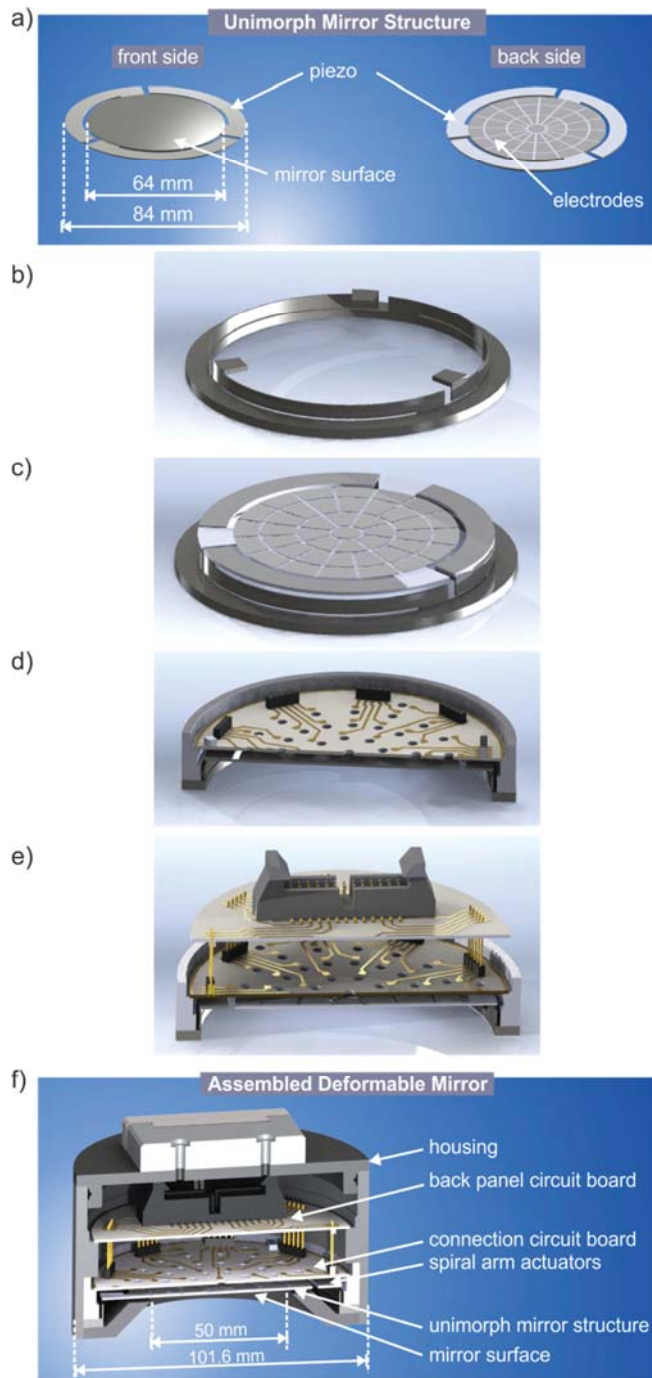


Fig. 4 a) unimorph mirror structure, b) mounting ring, c) mounted mirror structure, d) connection board on top of the connection board, e) back panel circuit board on top of the connection board, f) cross-sectional view of the assembled mirror

To facilitate the tip-tilt functionality of the mirror, steel segments which serve as passive layer are adhesively bonded to the spiral arms of the piezo structure. To bond the segments onto the arms we use a heat-curing low outgassing epoxy.

In a laminate consisting of two materials with different coefficients of thermal expansion (CTE), any changes of

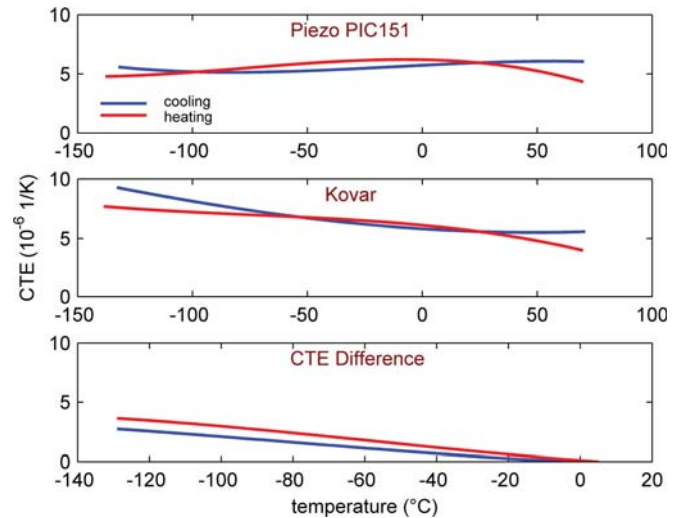


Fig. 5 Measurement of the thermal expansion coefficient (CTE)  
top: piezoelectric material middle: low-CTE nickel alloy Kovar  
bottom: CTE difference

ambient temperature will cause the laminate to bend due to the thermally induced stress (bimetallic effect). During operation, a deformable mirror can be exposed to environmental temperature changes. Therefore, mirror concepts are desirable which allow matching the CTE's of the employed materials. Due to the simple design of the proposed mirror structure and the possibility to select the passive layer from a wide variety of materials, our mirror concept allows to match the CTE's. Unfortunately, the CTE of most materials is not known very precisely, especially at cryogenic temperatures. Moreover, the CTE's of piezo ceramics can differ significantly from batch to batch. The manufacturer specifies the CTE of the employed piezo ceramic PIC151 to be in the range of  $4$  to  $8 \times 10^{-6} \text{ K}^{-1}$  whereas the coefficient of the selected glass material N-BK10 is stated as  $5.88 \times 10^{-6} \text{ K}^{-1}$ . These values are only mean values, approximately valid for the temperature range of  $0 \text{ }^\circ\text{C}$  to  $100 \text{ }^\circ\text{C}$ .

Equally important as matching the CTEs of glass and piezo is to match the CTEs of the piezo element and the material of the mechanical support ring (see Fig. 4b), because otherwise the deformable mirror will bulge if compressive stress arises. Therefore, we have conducted a series of low-temperature CTE measurements to obtain more precise values and to identify optimum material combinations. It turned out that the low-CTE nickel-alloy Kovar (material number 1.3917) represents the best trade-off over a large temperature range (see Fig. 5). At room temperature the CTE difference between piezo and steel is below  $10^{-7} \text{ K}^{-1}$ . For lower temperatures the difference increases almost linearly, at  $-120 \text{ }^\circ\text{C}$  the difference is  $2.5$ - $3.5 \times 10^{-6} \text{ K}^{-1}$ .

In the course of the development process various design variables, such as material properties and mirror dimensions, e.g. the thicknesses of the piezo layer and the glass layer, have been optimized by means of analytical and numerical calculations. Figure 6 shows the achievable defocus stroke for piezo/glass laminates depending on the thickness of the individual layers at the maximum voltage of  $400 \text{ V}$ . This

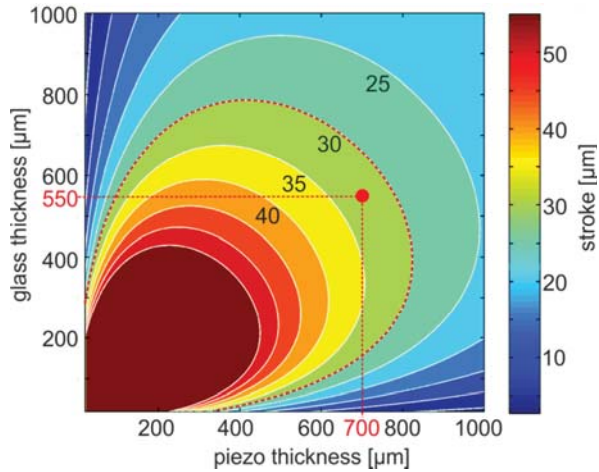


Fig. 6 Defocus stroke of the laminate as a function of individual layer thickness for an applied voltage of 400 V

voltage is determined by the maximum applicable electric field strength of the piezo material. The red dot represents the selected thickness configuration. In our mirror design, the thickness of the laminate has been chosen to permit a defocus peak-to-valley deformation of  $\sim 30 \mu\text{m}$ . It can be seen from Fig. 6 that higher stroke could be achieved by using thinner piezo and glass discs. However, the stiffness of the laminate is proportional to the third power of its thickness. A thin laminate becomes a very floppy structure with poor flatness in the unpowered state. The selected thicknesses reflect a compromise between high stroke and sufficient initial flatness.

Figure 4 shows CAD illustrations of the unimorph laminate along with the modular mirror construction and a cross sectional view of the final mirror assembly. The mechanical support of the mirror is designed to withstand vibrations and shocks which may be imposed on the assembly during the start of the launcher vehicle. The following list depicts some of the mirror's design features:

- 44 electrodes
- overall diameter of mirror structure:  $\text{Ø } 84 \text{ mm}$
- clear optical aperture:  $\text{Ø } 50 \text{ mm}$
- piezo layer thickness:  $700 \mu\text{m}$
- glass layer thickness:  $550 \mu\text{m}$

### III. MIRROR CHARACTERIZATION

We have conducted extensive numerical FEM calculations to estimate the performance of the proposed design. These investigations include the reproduction capability of low-order Zernike modes and the analysis of the mirror's eigenmodes and frequency responses.

#### A. Generation of Zernike Modes

The reproduction of Zernike modes up to the 12th order has been calculated via finite element modeling and is shown in Fig. 7. The amplitudes are either limited by the maximum allowed voltage of 400 V, or by the residual wavefront error if it exceeds  $\lambda/14$  (Maréchal criterion) for  $\lambda = 1064 \text{ nm}$ . Generally, the wavefront error increases with increasing amplitude, hence the Maréchal criterion ensures diffraction-limited Zernike reproduction.

According to the results in Fig. 7, diffraction-limited Zernike modes with strokes of up to  $35 \mu\text{m}$  in defocus mode and around  $3 - 10 \mu\text{m}$  for higher order modes can be achieved. The tip-tilt amplitudes exceed  $70 \mu\text{m}$ , possibly rendering additional tip-tilt stages superfluous.

#### B. Dynamic Behaviour

An FEM frequency response analysis revealed that the first eigenfrequencies occur at approximately 200 Hz. The positions of the eigenfrequencies are directly related to the flexural rigidity of the mirror structure. They can be shifted towards higher values by increasing the stiffness. An eigenmode analysis showed that the first frequencies are mainly determined by the mechanical properties of the three spiral arms. Accordingly, by stiffening merely the arms we can adapt the mirror to achieve higher actuation frequencies without affecting the central disc. This would solely entail a reduction of the tip-tilt amplitude.

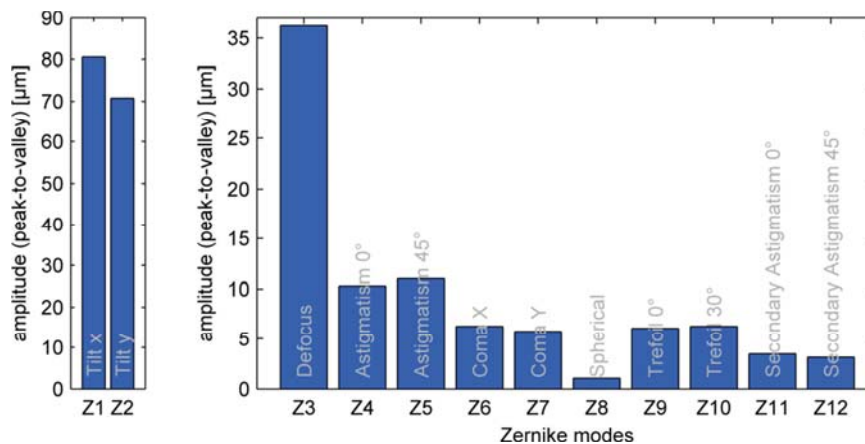


Fig. 7 Numerically calculated low order Zernike-amplitudes for the presented mirror configuration

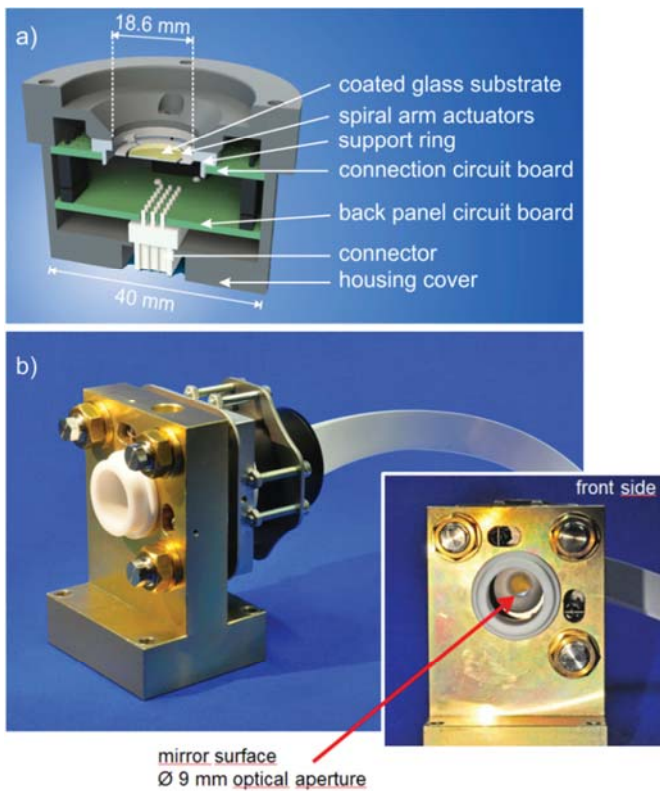


Fig. 8 a) Cross-section of the small-scale mirror prototype,  
b) Photo of mounted prototype mirror assembly

#### IV. SMALL SCALE MIRROR PROTOTYPE

To validate the numerical and analytical predictions for the proposed mirror design, a smaller-sized prototype mirror was fabricated and characterized (see Fig. 8) preserving the essential characteristics of the larger mirror concept. Analog to the preceding chapter, the following list depicts design features for the smaller-sized mirror:

- 35 electrodes
- overall diameter of mirror structure:  $\varnothing$  18.6 mm
- clear optical aperture:  $\varnothing$  9 mm
- piezo layer thickness: 200  $\mu$ m
- glass layer thickness: 100  $\mu$ m

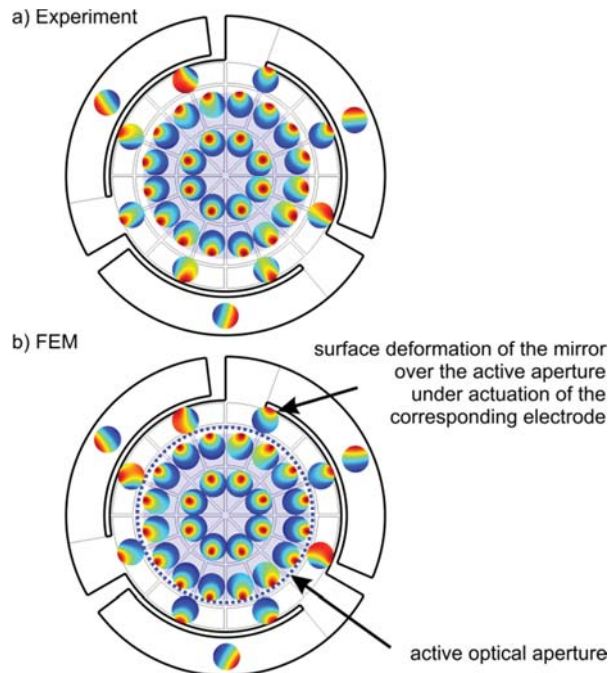


Fig. 9 Influence functions of the mirror electrodes. Shown is the deformation that results if a single electrode is supplied with a voltage of 100 V. The false-color elevation plots representing the mirror deformations are plotted at the position corresponding to the activated electrode. a) Experimentally measured deformations, b) FEM simulation

#### A. Influence Functions

The spatial characteristics of deformable mirrors are fully determined by the influence functions, i.e. the deformation of the whole mirror surface in response to the actuation of each individual electrode. Figure 9 shows the measured influence functions of all electrodes as well as the numerically calculated ones. The measured surface profiles are in very good agreement with our numerical predictions.

#### B. Generation of Zernike Modes

Figure 10 shows experimentally measured and numerically calculated Zernike amplitudes of the mirror prototype (Fig. 8). The surface figure was analyzed using a phase-stepping interferometer. The experimental results compare well with the

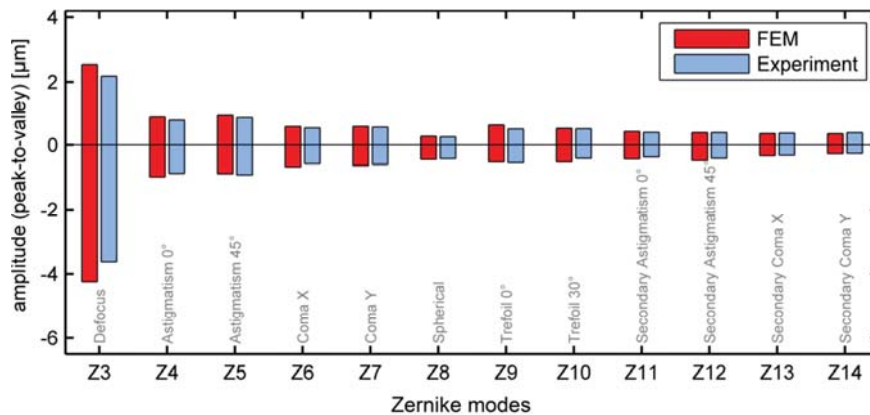


Fig. 10 Comparison between calculated and measured Zernike amplitudes generated by the smaller-sized prototype mirror

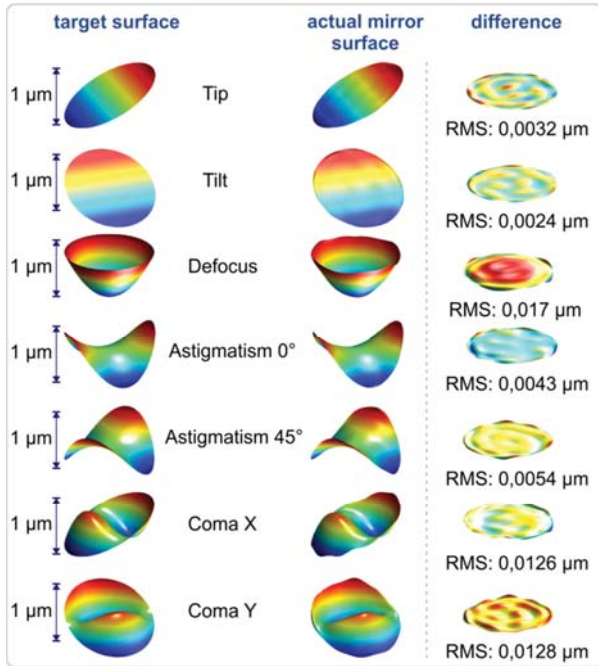


Fig. 11 Comparison between the target mirror surface and the actual mirror surface along with the residual surface error

simulated values obtained by FEM calculations. The maximum deviation is below 14 %. The good agreement validates the applicability of the numerical model. This is also proven by Fig. 11 which shows the actual mirror surface for several

targeted low-order Zernike modes with a stroke of 1 μm. The difference between target and actual surface is expressed by the residual RMS error. The residual RMS wavefront error remains below  $\lambda/30$ , exceeding the  $\lambda/14$  Maréchal criterion and thus ensuring diffraction-limited imaging.

### C. Laser Power Handling Capability

Our deformable mirror was originally invented for the use in high-power lasers. It has been experimentally confirmed that it withstands at least 7700 W of incident irradiation (1 μm wavelength) corresponding to an intensity of 560 kW/cm<sup>2</sup> in continuous-wave mode. The experimental setup is shown in Fig. 12. For this experiment, the smaller-sized mirror has been incorporated in a V-shaped high-power thin disc laser resonator. During laser operation, no mirror deformation or significant rise in temperature was detected.

The high power handling capability enables the use of our mirror to control the wavefront of a Laser Guide Star (LGS) adaptive optics system. Light from such an artificial guide star is used to measure the wavefront aberrations caused by atmospheric turbulences in a cone next to the science object. By controlling the wavefront of the LGS beam, one can improve the performance of such an LGS system.

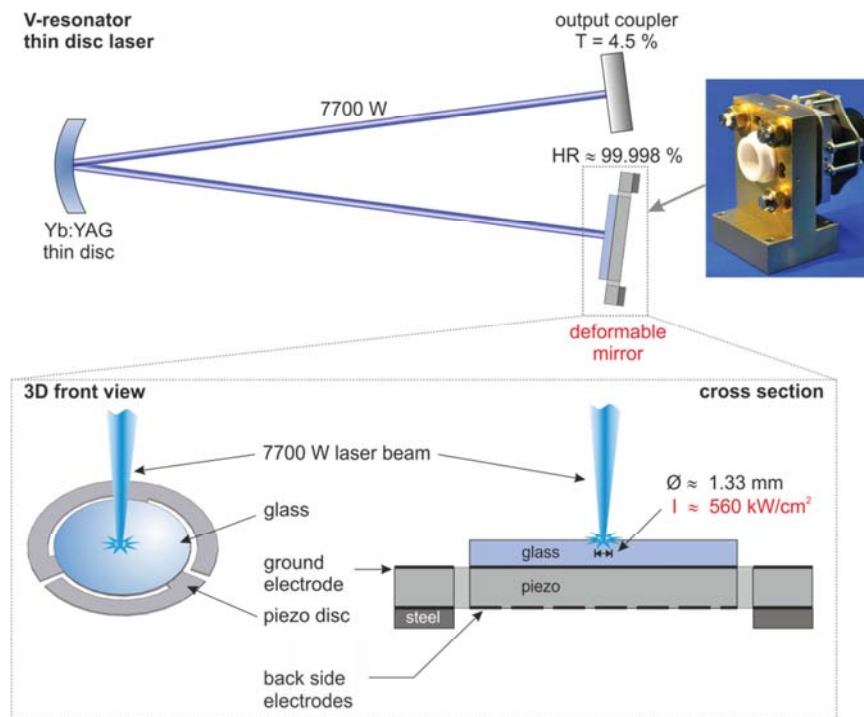


Fig. 12 Experimental setup to verify the power handling capability of the deformable mirror

## V. CONCLUSION

We have presented a new concept for an adaptive deformable mirror. Its characteristics suggest the use in applications which require correction of low spatial frequency, large amplitude aberrations, and operation at medium temporal correction bandwidth. The feasibility of the concept has been validated by manufacturing and testing of a smaller-sized prototype mirror.

The flexible concept allows scaling the mirror aperture within one order of magnitude. It is possible to render the mirror insensitive to thermal fluctuations by smart selection of materials for the passive layers. We have demonstrated that the mirror is able to withstand high power laser irradiance.

Applications of the mirror could be the use as a woofer in a woofer-tweeter system or the correction of non-perfect large telescope optics. Furthermore, the excellent power handling capability suggests using the mirror to control the wavefront of laser beams in applications incorporating high-power lasers.

## VI. ACKNOWLEDGMENT

The authors gratefully acknowledge support for the work presented by the European Space Agency under contract number 4000104030/10/NL/EM.

## REFERENCES

- [1] Allen, L., Angel, J. R. P., Mongus, J. D., Rodney, G. A., Shannon, R. R., Spoelhof, C. P. , "The Hubble Space Telescope optical systems failure report," NASA Report, (1990)
- [2] Beckers, J. M. "Adaptive optics for astronomy - Principles, performance, and applications," Annual review of Astronomy and Astrophysics. Vol. 31, p. 13-62. (A94-12726 02-90)
- [3] Hardy, J. W. "Adaptive Optics for Astronomical Telescopes," Oxford University Press (1998)
- [4] Poyneer, L. A., Bauman, B., Cornelissen, S., Isaacs, J., Jones, S., Maxintosh, B. A., Palmer, D. W., "The use of a high-order MEMS deformable mirror in the Gemini Planet Imager," Proc. SPIE, 7931 (2011)
- [5] Kudryashov, A., Shmalhausen, V., "Semipassive bimorph flexible mirrors for atmospheric adaptive optics applications," Optical Engineering, Vol. 35, p. 3064-3072 (1996)
- [6] Verpoort, S. and Wittrock, U. "Actuator patterns for unimorph and bimorph deformable mirrors," Applied Optics, Vol. 49, No. 31, G37-G46 (2010)